PAPER • OPEN ACCESS

Quantum size effects of small, size-selected and deposited CoRh clusters on Ni

New Journal of Physics
The open access journal at the forefront of physics

Deutsche Physikalische Gesellschaft DPG
IOP Institute of Physics

Published in partnership with: Deutsche Physikalische Gesellschaft and the Institute of Physics

OPEN ACCESS

RECEIVED
3 June 2016

REVISED
4 September 2016

ACCEPTED FOR PUBLICATION
13 October 2016

PUBLISHED
4 November 2016

PAPER

Quantum size effects of small, size-selected and deposited CoRh clusters on Ni

T Beeck[1], **I Baev**[1], **K Chen**[2], **S Palutke**[1], **W Wurth**[3,4] **and M Martins**[1]

[1] Physics Department, University of Hamburg, Luruper Chaussee 149, D-22761 Hamburg, Germany
[2] Institute of Physics II, University of Cologne, Zülpicher Straße 77, D-50937 Cologne, Germany
[3] Physics Department and Center for Free-Electron Laser Science, University of Hamburg, Luruper Chaussee 149, D-22761 Hamburg, Germany
[4] DESY Photon Science, Notkestraße 85, D-22607 Hamburg, Germany

E-mail: michael.martins@desy.de

Keywords: XAS, XMCD, deposited clusters, nanoscale magnetism, chemical reactivity

Abstract

The electronic, chemical and magnetic properties of *in situ* prepared, mass-selected and deposited Co_xRh_y alloy clusters with up to five atoms per cluster have been studied by means of x-ray absorption and x-ray magnetic circular dichroism spectroscopy. The clusters were supported on a remanently magnetized Ni film. The cluster properties exhibit strong size and composition dependent effects. By alloying of pure $Co_{1,2}$ adatoms and dimers with Rh the chemical reactivity towards oxygen is significantly enhanced for specific compositions. The oxidation of the alloyed clusters strongly affects the magnetic properties which results in a reduction of the orbital and spin magnetic moments. The exchange coupling between the oxidized Co atoms and the Ni surface exhibits a size and a composition dependent oscillation between antiferromagnetic and ferromagnetic coupling.

1. Introduction

The size dependent investigation of nanoparticle and cluster properties is a very active research area. The closing gap between industrial application and fundamental research certainly is one reason of the strong interest. In divisions like electronics, magnetism, optics, mechanics and medical health care, devices and particles are scaled down and redesigned to the scale of several tens to sub-nanometers. In this region finite size effects become crucial and along with this size dependence unexpected material properties arise which can strongly differ compared to the bulk. For magnetic materials, it has been shown that reducing the dimensionality leads to enhanced magnetic moments compared to the bulk [1, 2]. In the bulk, 4d transition metals like rhodium exhibit no magnetism, although being close to fulfill the Stoner criterion for ferromagnetism. Cox and coworkers showed that the reduction in size, down to a Rh cluster size of less then 60 atoms, led to superparamagnetism and enhanced magnetic moments of the clusters [3, 4].

In modern high density magnetic recording applications alloys of ferromagnetic 3d transition metals with 4d or 5d transition metals are used. The aim is to overcome the superparamagnetic limit by increasing the orbital magnetic moment and the magnetic anisotropy energy with the help of the strong spin–orbit interaction of the 4d/5d elements. Since Rh clusters do exhibit a considerable magnetic moment, it is reasonable to consider 3d-Rh alloys as promising magnetic storage materials.

Alloying of Co with Rh has been studied experimentally and theoretically in a variety of systems, e.g. alloys [5, 6], multilayers [7, 8], nanoparticles [9–14] and clusters [15–19]. For these systems an induced magnetic moment on the Rh site was reported, strongly depending on the magnetic environment. Calculations on free neutral [15–18] as well as experiments on free ionic [19] CoRh clusters showed that the orbital and spin magnetic moments can be either enhanced or reduced if compared to the pure Co clusters. These non-monotonous trends are linked to the complex interplay between the cluster size, the geometry and its composition. However, so far no systematic studies on deposited, small and mass-selected CoRh clusters have been performed. The

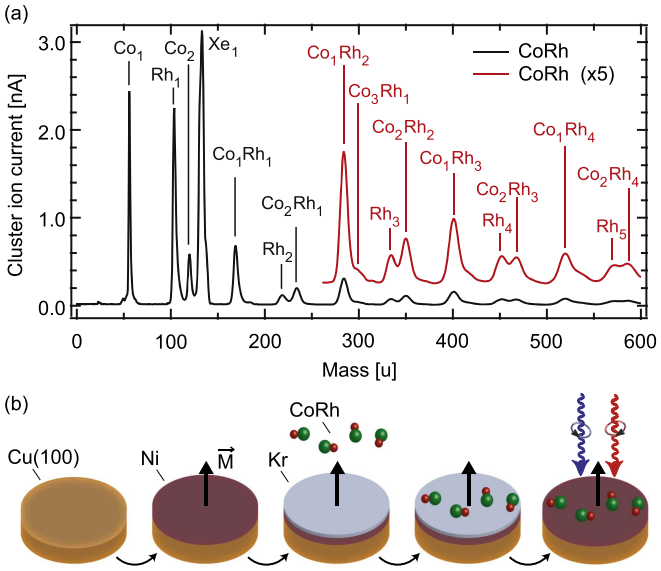

Figure 1. (a) CoRh mass spectrum recorded at the sample position. All species prepared are clearly resolved. (b) Illustration of the sample preparation with Ni film evaporation and soft landing procedure of the Co_xRh_y clusters.

deposition is crucial from a technical point of view but typically changes the cluster properties with respect to the gas phase unless the cluster-substrate interaction is actively suppressed [20].

In this paper, experiments on mass-selected Co_xRh_y alloy clusters deposited on a magnetized Ni/Cu(100) surface are presented. The clusters are systematically varied in size atom by atom up to the five atomic Co_2Rh_3 cluster and investigated by x-ray absorption (XAS) spectroscopy techniques. The focus of the experiment is to study the evolution of the electronic, chemical and especially magnetic properties of the CoRh 3d/4d alloy clusters in a size and composition dependent manner on the Ni surface.

2. Experiment

The Co_xRh_y cluster samples have been investigated at the BESSY II synchrotron light source using the soft x-ray UE52-SGM beamline [21]. The XAS and x-ray magnetic circular dichroism (XMCD) spectroscopy techniques are perfectly suited to study the electronic, chemical and magnetic sample characteristics in an element-selective way. With XAS, the unoccupied electronic states and the chemical environment of the cluster Co atoms were probed by exciting 2p $\rightarrow$ 3d transitions at the Co $L_{2,3}$-edges. Using the circular polarized light of the beamline, the magnetic properties at the Co and Rh sites (Rh $M_{2,3}$-edges, 3p $\rightarrow$ 4d) were examined by XMCD.

All cluster samples were produced *in situ* using a UHV-cluster source [22] with mass-selecting dipole magnet. The cluster source was operated with 30 keV Xe^+ ions to sputter a $Co_{0.5}Rh_{0.5}$ target. All positively charged sputter fragments are accelerated to an electrostatic lens by setting the target potential to +500 V. The lens guides the clusters to the dipole magnet offering a resolution of $m/\Delta m \approx 50$. Behind the dipole magnet, the mass-selected clusters, shown in figure 1(a), are first decelerated to an energy of about 1 eV $atom^{-1}$ and in the following deposited via a soft-landing scheme [23, 24] on a pseudomorphic 20–30 monolayer (ML) Ni/Cu (100) surface (figure 1(b)). In this size regime, the Ni film shows a remanent out-of-plane magnetization if aligned by an external magnetic field [25, 26]. The clusters are aligned parallel to the magnetic orientation of the film by exchange coupling. The Kr buffer gas (≈8–9 ML) adsorbed for the soft landing process was removed by annealing the sample from 35 K base temperature to about 100 K. With the used scheme, fragmentation of the deposited clusters is effectively suppressed [27]. In order to avoid agglomeration and inter cluster interaction, the cluster coverage was chosen to 0.03 ML. For all studied samples, the here described surface preparation process was carried out at a base pressure of about 3×10^{-10} mbar.

The XAS and XMCD measurements were carried out in the total electron yield (TEY) detection mode at a base pressure of 2×10^{-10} mbar. The resolving power $E/\Delta E$ of the beamline at the Co $L_{2,3}$- and the Rh $M_{2,3}$-edges was around 2300 and 2500, respectively. Due to the lower cross section at the Rh $M_{2,3}$-edges, the exit slit was opened from 100 to 150 μm with respect to the Co measurements. Moreover, due to time constraints, the step width was increased from 0.2 to 0.5 eV. Sufficient statistics were obtained with counting times of 4 s per data point for left and right circular photon polarization. In order to check the Ni film thickness and to

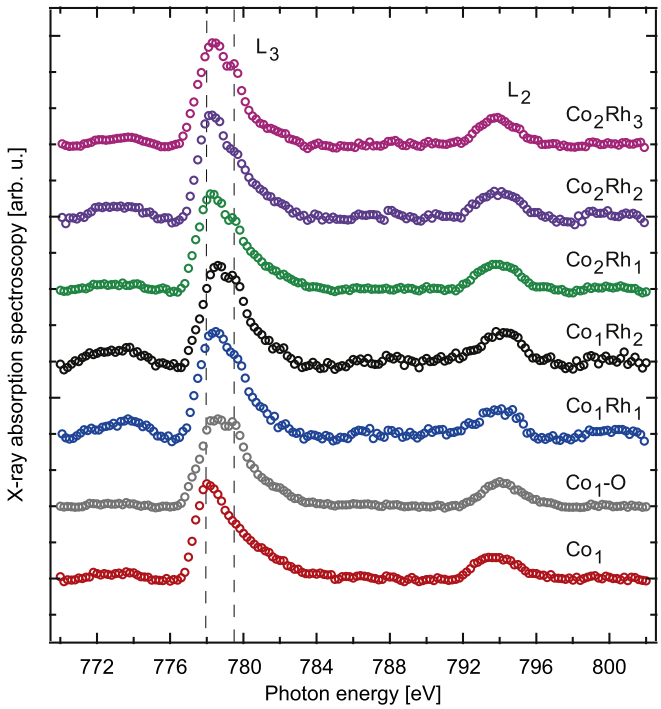

Figure 2. The XAS spectra of Co_xRh_y clusters on Ni/Cu(100) are shown at the Co $L_{2,3}$-edges. The L_3-edge main peak shows two distinct features indicated by the dashed lines. While the left line does not fit for all species, the right perfectly matches. The Co_1–O spectrum was already published in [28].

normalize the magnetic cluster signal to the Ni magnetization, the Ni and Cu XAS signal at the $L_{2,3}$-edges were recorded too.

3. Results and discussion

3.1. Chemical properties

Figure 2 shows XAS spectra at the Co $L_{2,3}$-edges of two Co_1 adatom as well as Co_1Rh_y and Co_2Rh_y cluster preparations. All spectra were normalized to the incoming photon flux through division by the TEY signal of the last refocussing mirror of the beamline. In a next step, the normalized spectra were subtracted by a fifth order polynomical fit representing a combination of the smooth substrate background and the continuum-steps at the $L_{2,3}$-edges. Different signal to noise ratios in figure 2 correspond mainly to the change of the Co content of the individual cluster species. At the bottom, the measured and well known Co_1 adatom spectrum is presented [28, 29]. The main peak of the Co L_3-edge at 778.0 eV (left dashed line) exhibits no fine structure in contrast to the alloy clusters. There, a side peak at a constant energy of 779.5 eV is observed (right dashed line), independent of cluster size and composition. In contrast, a clear chemical shift of the main peak to higher excitation energies is present.

The fine structure of the alloy clusters can be assigned to an increased chemical reactivity towards oxygen rather than resulting from alloying Co with Rh. This can be inferred from the shown Co_1–O spectrum [28], representing the oxidized Co_1 adatom and thus, clearly correlating the side peak to the presence of oxygen. Even a broadening on the low photon energy side, in CoO bulk, layer and nanoparticles [30–32] seen by a small peak at 776.6 eV, is visible. Similar oxidation effects have been reported already for size selected CoPd and CoPt alloy clusters on Ni [28, 29]. The fully oxidized Co_1–O sample was prepared in [28] by introducing a waiting time of 60 min. between the magnetization of the Ni film and the deposition of the Kr buffer layer. This is in contrast to the here shown CoRh samples, exhibiting no waiting time. The missing CoRh oxides in the collected mass spectra (figure 1(a)) show that the oxidation is surface mediated. Moreover, the process must be related to the soft-landing scheme since no changes of the XAS signal were present during the measurements. However, the mechanism of the oxidation process is still not fully understood and made it impossible to study the pure CoRh cluster properties. Nevertheless, the similar preparation of the clusters allows a size and composition dependent comparison among themselves.

The varying height of the side peak can be used to estimate the fraction of oxidized clusters in the preparations. Thus, the peak height of Co_1–O has been normalized to 1 and to 0 for the non-oxidized Co_1

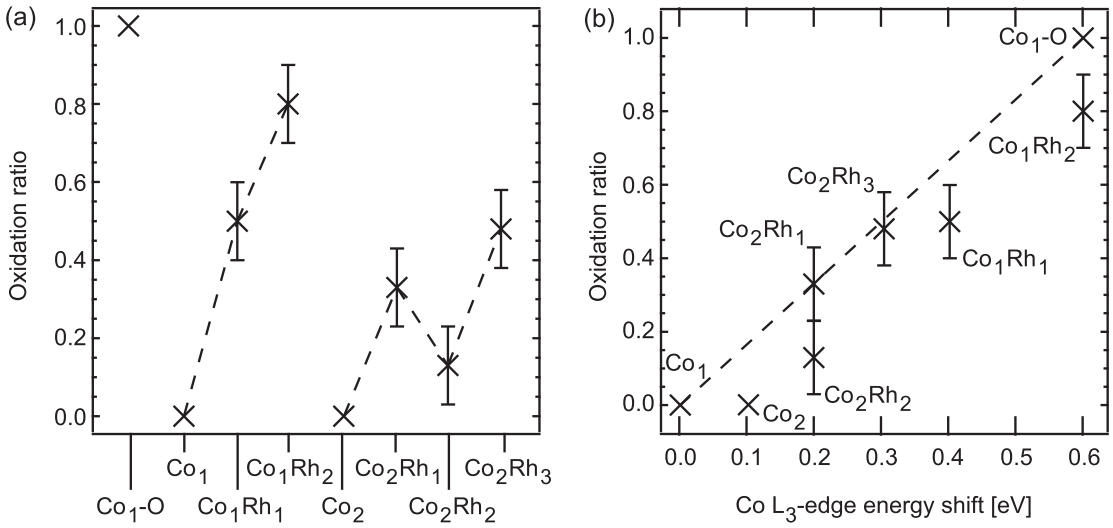

Figure 3. (a) The oxidation ratio for the pure Co and CoRh alloy clusters are shown. For instance, every second Co_1Rh_1 dimer of the deposited ensemble is oxidized. (b) The oxidation ratio against the relative L_3-edge main peak energy shift with respect to Co_1 is plotted. The dashed line indicates a linear oxidation relation. A general trend to higher excitation energies by alloying $Co_{1,2}$ with Rh can be seen. The Co_2 values are taken from earlier measurements [29].

adatom, respectively. Figure 3(a) shows the resulting oxidation ratio for each preparation. Since all CoRh preparations have been performed under similar conditions changes in the oxidation ratio directly reflect the size and composition dependent reactivity of the CoRh clusters. The Co_1Rh_y clusters exhibit a monotonous increase of the reactivity with increasing Rh content finally resulting in a nearly fully oxidized Co_1Rh_2 cluster. For Co_2Rh_y the reactivity is generally decreased if compared to Co_1Rh_y, indicating that the second Co atom might not be oxidized. Moreover, size and composition dependent effects are observed. Adding one Rh atom to Co_2Rh_1 reduces the reactivity by about 60%. In addition, with two additional Rh atoms it is enhanced by 30%.

The important role of the cluster geometry is demonstrated by the Co_1Rh_1 and Co_2Rh_2 cluster samples. Both species have the same alloying ratio but the reactivity of Co_2Rh_2 is reduced by a factor 4. Unfortunately, the low cluster coverage does not allow to gain information about the structure, e.g. by the EXAFS absorption signal.

3.2. Electronic properties

Although being dominated by the characteristic CoO fine structure, the XAS spectra of figure 2 contain information about the hybridization of the Co electronic states by alloying with Rh. Figure 3(b) shows the oxidation ratio of the Co_xRh_y clusters against the relative L_3-peak shift with respect to the Co_1 adatom. The dashed line implies a linear energy shift of the main peak if the fraction of the oxidized Co_1Rh_y clusters in the ensemble increases up to the full oxidized Co_1–O. All Co_1Rh_y samples clearly show a shift to higher photon excitation energies. On the one hand, this can be related to the increasing cluster size as has been shown already for free as well as deposited size-selected 3d transition metal clusters [33, 34]. There, initial and final state effects contribute to the enhanced excitation energy by an increased delocalization of the valence electrons. On the other hand, the shift can be addressed to an increased electron density at the Rh site as has been reported also for theoretical calculations on small CoRh clusters in the gas phase [16–18]. Thus, the reduced electron density at the Co site increases the 2p core level binding energy due to the weakened Coulomb repulsion of the electrons.

A similar shift to higher excitation energies under alloying with 4d/5d transition metals was reported also for small CoPd and CoPt alloy clusters on Ni/Cu(100) [28, 29]. Again, theoretical calculations on free alloy clusters confirm this trend for both systems and find an increased electron density on the 4d/5d site [35, 36]. However, for the CoPt clusters an increased electron density at the Co atoms was proposed, leading to the observed catalytic oxidation reaction. The complex interplay between the intra-cluster and cluster-substrate interaction, leading on Ni with a high density of states at the Fermi level to a more complex hybridization of the electronic states as in the gas phase, together with the not yet fully understood oxidation process makes it difficult to address the driving catalytic atomic sites.

The Co_2Rh_y clusters show a similar but smaller increase of the Co binding energies upon alloying. In contrast to the Co_1Rh_y clusters, the contributions to the higher binding energy upon alloying and oxidation could not be determined since the Co_2 dimer on Ni does not oxidize in the used preparation scheme. Nevertheless, the energy shift of about 0.2 eV is in the order of the observed increase with cluster size [34].

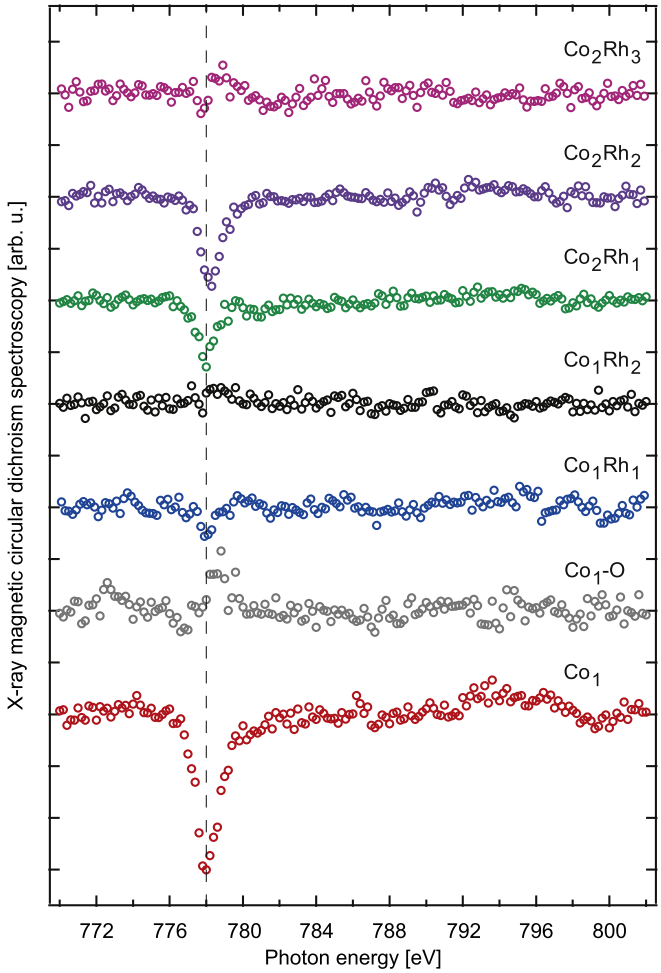

Figure 4. The XMCD signals of the different Co_xRh_y clusters on Ni/Cu(100) are shown at the Co $L_{2,3}$-edges. The dashed line is a guide for the eye and centered at the Co_1 L_3-edge dichroism signal at 778.0 eV. Note the XMCD sign change at the Co_1–O, Co_1Rh_2 and Co_2Rh_3 L_3-edge.

3.3. Magnetic properties

While the XAS spectra in figure 2 only contain spin-averaged information, the XMCD spectra shown in figure 4 hold information about the spin-resolved unoccupied density of states. The spectra show the difference of the absorption signals for left and right circular polarized light. Using the so-called magneto-optical sum rules [37, 38], the spectra can be related to the element-specific orbital (m_l) and effective spin ($m_s^{\mathrm{eff}} = m_s + 7m_t$) magnetic moments. The effective spin magnetic moment represents the spin moment (m_s) together with the magnetic dipole moment (m_t) which accounts for the asphericity of the spin moment distribution. In the following, the effective spin moment m_s^{eff} will be denoted for simplicity as spin moment m_s.

In figure 4, the Co_1 adatom exhibits the strongest dichroism signal of all measurements. Its orbital and spin magnetic moment has been measured and reproduced before [28, 29] and serves as reference for the accuracy of the preparations and measurements performed. The values in table 1 show that the evaluated magnetic moments are in good agreement to the former results.

A comparison between the Co_1 and the Co_1–O spectra shows a change of sign in the dichroism signal as has been already reported earlier [28]. The change in sign is related to a different coupling to the underlying Ni substrate, meaning ferromagnetic coupling for Co_1 and antiferromagnetic coupling for Co_1–O respectively. The different coupling of the oxidized adatom is important since alloying of Co_1 and Co_2 with Rh made it impossible to study non-oxidized clusters. Thus, the comparison of the calculated oxidation ratio with the evaluated magnetic moments and the observed coupling to the Ni substrate holds information how the oxidation of the Co_xRh_y clusters effects their magnetic properties.

Table 1 and figure 5(a) show that adding one Rh atom to the Co_1 adatom results in a 70% decrease of the total magnetic moment. The XMCD signal gives a small ferromagnetic coupling to Ni, and the enhanced activity due to Rh alloying results in half of the clusters being oxidized. Further alloying by one Rh atom to Co_1Rh_2 flips the XMCD signal at the L_3-edge to positive values and antiferromagnetic coupling. Note that the XMCD signal is

Table 1. By sum rule analysis evaluated orbital, spin and total magnetic moments per number of d-holes and in units of μ_B are given for Co_xRh_y alloy clusters on Ni/Cu(100). The estimated content of oxidized clusters per sample is given with an error of ±10%. The magnetic moments of the full oxidized Co_1 spectrum have been taken from [28] and for the Co_2 dimer from [29].

Sample	Oxide (%)	m_l (μ_B/h_d)	m_s^{eff} (μ_B/h_d)	m_l/m_s^{eff}
Co_1	0	0.11 ± 0.03	0.42 ± 0.06	0.26 ± 0.05
Co_1	100	−0.01 ± 0.005	−0.03 ± 0.01	0.34 ± 0.11
Co_2	0	0.12 ± 0.03	0.57 ± 0.04	0.20 ± 0.03
Co_1Rh_1	50	0.04 ± 0.01	0.11 ± 0.03	0.32 ± 0.07
Co_1Rh_2	80	−0.02 ± 0.01	−0.11 ± 0.03	0.19 ± 0.05
Co_2Rh_1	33	0.08 ± 0.01	0.26 ± 0.04	0.30 ± 0.06
Co_2Rh_2	13	0.13 ± 0.04	0.47 ± 0.10	0.28 ± 0.08
Co_2Rh_3	48	−0.01 ± 0.005	−0.04 ± 0.01	0.18 ± 0.06

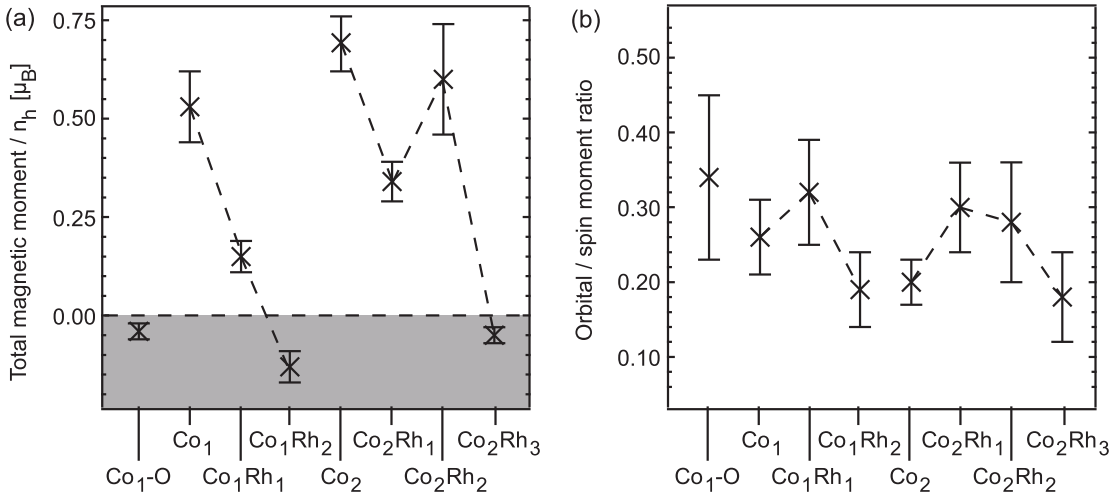

Figure 5. (a) The total magnetic moment of pure $Co_{1,2}$ and alloy Co_xRh_y clusters are plotted. A negative magnetic moment (gray area) indicates anitferromagnetic coupling between the cluster and the magnetic Ni film. (b) The m_l/m_s^{eff} ratio of each species is shown. The Co_2 values in both plots are taken from [29].

shifted by 0.5 eV similar to Co_1–O. However, compared to Co_1–O the total moment is tripled with the spin moment m_s^{eff} increasing twice as much than the orbital moment. As a consequence the m_l/m_s^{eff} ratio decreases.

The high oxidation ratios, e.g. 80% for the Co_1Rh_2 clusters, make it important to address whether the different coupling for Co_1Rh_1 and Co_1Rh_2 is mainly driven by Rh or oxygen. While the L_3 energy shift is most likely due to the oxygen, it was not possible to disentangle the different Co–O, Co–Rh contributions in the XMCD spectra, for example by a linear combination model between ferro- and antiferromagnetic coupled clusters as applied in [28]. Thus, XMCD measurements at the Rh $M_{2,3}$-edges were performed for the antiferromagnetic coupled Co_1Rh_2 clusters. In figure 6, the XAS and XMCD signals are shown respectively. No magnetic contribution of the Rh atoms is observed in contrast to induced moments in CoRh thin films [5], exchange coupled multilayers [8], nanoparticles [9, 13] and the nearest neighbors of Co adatoms on Rh(111) [39].

The Co_2 dimer has a comparable orbital moment and an increased spin moment with respect to the adatom [29]. Thus, the total magnetic moment is increased while the ratio decreases by about 25%, as depicted in figures 5(a) and (b). Alloying the Co_2 dimer with a Rh atom again leads to an enhanced reactivity for the Co_2Rh_1 cluster. The evaluated oxidation ratio is nearly half the value of Co_1Rh_1 and could be a hint for a non-oxidized second Co atom. Comparing the magnetic moments of Co_2Rh_1 and Co_1Rh_1, the observed increase of the Co_2Rh_1 orbital and spin moment by a factor 2 and 2.5, respectively, strengthens this point. However, with respect to the pure dimer both magnetic moments are reduced by 35% and 55%. Thus, the total moment is halved.

Having seen already a distinct size dependent effect when adding a second Rh atom to Co_1Rh_1, a similar effect appears for the transition from Co_2Rh_1 to Co_2Rh_2. The reactivity of the clusters decreases and only a small fraction is oxidized (figure 3(a)). Compared with the observation for Co_1Rh_y clusters in figure 5(a), this

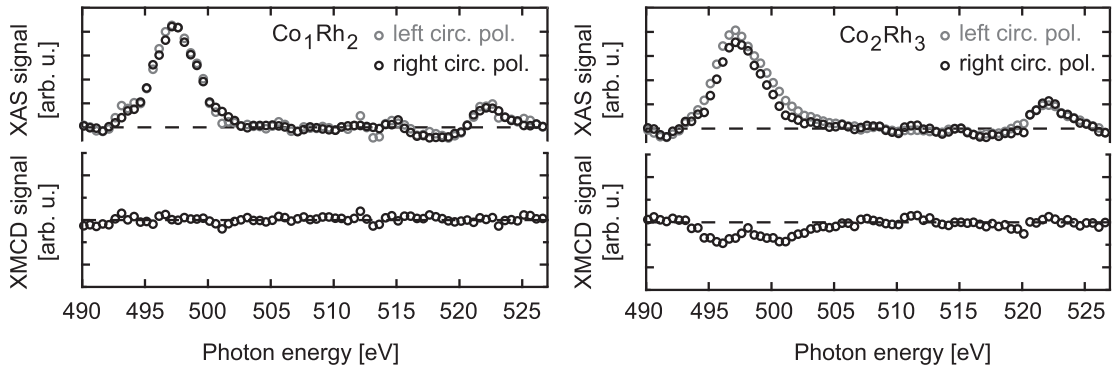

Figure 6. The XAS and XMCD spectra at the Rh $M_{2,3}$-edges of Co_1Rh_2 and Co_2Rh_3 on Ni/Cu(100) are presented. The Co_1Rh_2 clusters exhibit no dichroism. In contrast, for Co_2Rh_3 a magnetic contribution of the Rh atoms is found.

interestingly leads to an increase of the Co_2Rh_2 m_l and m_s^{eff} values, both increasing by 40% and 45% with respect to Co_2Rh_1. Exclusively for all Co_xRh_y clusters investigated, the Co_2Rh_2 orbital moment is enhanced by alloying. The magnetic moments are of comparable size to the pure Co_1 and Co_2. Similar to the Co_1Rh_2 clusters, no XMCD signal at the Rh $M_{2,3}$-edges was observed.

By adding three Rh atoms to the Co_2 dimer the size-dependence of the Co_2Rh_y total magnetic moments is revealed beautifully, as can be seen in figure 5(a). As for the Co_1Rh_2 clusters, having likewise an alloying ratio above 50%, an antiferromagnetic, positive Co L_3-edge contribution is observed in the XMCD spectrum of figure 4 accompanied with a sign change for the magnetic moments. A detailed study of the Co_2Rh_3 XMCD spectrum shows that there seems to be a small ferromagnetic contribution in addition. A similar effect is implied in the Co_1Rh_2 XMCD signal. Surprisingly, the Co_2Rh_3 XMCD spectrum at the Rh $M_{2,3}$-edges, shown in figure 6, exhibits a dichroism signal. The negative signal implies an antiparallel coupling between the magnetic moments of the Rh and Co atoms (compare to figure 4) and a parallel coupling between the magnetic moments of Rh and Ni. Assuming that the clusters prefer a certain structure on the surface, this points to a complex, non-collinear spin structure [40, 41]. The evaluated small orbital and spin magnetic moments strengthen this interpretation. The Co_2Rh_3 cluster is showing the highest reactivity of all Co_2Rh_y clusters. Approximately half of the clusters are oxidized. Compared to the other antiferromagnetic coupled Co_1Rh_2 cluster, the orbital and spin moments are reduced drastically by about 50%. The ratio of the magnetic moments stays unchanged.

A detailed study of the ratios of the magnetic moments in figure 5(b) reveals a certain dependency for Co_1Rh_y and Co_2Rh_y clusters. Compared to the pure Co_1 and Co_2, the ratios are enhanced if the alloying ratio is $\leqslant$50%. Further alloying to $>$50% lowers the ratios to a minimum. For the smaller alloying ratios (Co_1Rh_1, Co_2Rh_1) this is related to a faster decreasing spin moment while for the higher alloying ratios (Co_1Rh_2, Co_2Rh_3) the orbital moment is suppressed. An exception makes the Co_2Rh_2 cluster as described before.

4. Summary and conclusions

In summary, we have performed XAS and XMCD studies on mass-selected Co_xRh_y clusters deposited on a magnetized Ni/Cu(100) surface. The clusters were systematically varied in size atom by atom up to the five atomic Co_2Rh_3.

Alloying with Rh leads to an enhanced chemical reactivity towards oxygen for each Co_xRh_y preparation. The photon excitation energy of the alloyed Co atoms is increased which corresponds to a reduced electron density at the Co site. Depending on their size and composition, the magnetic moments of all alloyed clusters are reduced by oxidation and exhibit an oscillatory ferro-/antiferromagnetic transition of the exchange coupling between the Co atoms and the Ni surface. The Co_1Rh_y cluster magnetic moments are of comparable size and with respect to Co_1 suppressed to about 20% of the orbital and 25% of the effective spin magnetic moment. For Co_2Rh_y, higher magnetic moments than for Co_1Rh_y are found together with a reduced oxidation ratio. Thus, the second Co atom does not seem to be oxidized. An exception is given by the Co_2Rh_3 cluster with the lowest magnetic moments of all alloy clusters. The dichroism signals of the Co and Rh atoms show an antiferromagnetic coupling for Co and a ferromagnetic for Rh with respect to the Ni surface, leading to a possible non-collinear spin structure. The orbital to spin moment ratios show a similar dependency for Co_1Rh_y and Co_2Rh_y. Alloying ratios less than or equal to 50% lead to enhanced ratios compared to $Co_{1,2}$, while further alloying to greater than 50% decreases the ratios. An exception is given by Co_2Rh_2, showing an oxidation ratio below 20% and magnetic moments in the order of $Co_{1,2}$.

Acknowledgments

We thank the BESSY II beamline staff, namely H Pfau and F-X Talon, for their logistic assistance. Financial support by the Deutsche Forschungsgemeinschaft (DFG) through SFB 668 is gratefully acknowledged.

References

[1] Billas I M, Châtelain A and de Heer W A 1994 *Science* **265** 1682–4
[2] Gambardella P *et al* 2003 *Science* **300** 1130–3
[3] Cox A J, Louderback J G and Bloomfield L A 1993 *Phys. Rev. Lett.* **71** 923
[4] Cox A J, Louderback J G, Apsel S E and Bloomfield L A 1994 *Phys. Rev.* B **49** 12295
[5] Harp G R, Parkin S S P, O'Brien W L and Tonner B P 1995 *Phys. Rev.* B **51** 12037
[6] Ostanin S, Popescu V and Ebert H 2001 *J. Phys.: Condens. Matter* **13** 3895
[7] Dinia A, Zoll S, Gester M, Stoeffler D, Jay J, Ounadjela K, van den Berg H and Rakoto H 1998 *Eur. Phys. J.* B **5** 203
[8] Tomaz M A, Mayo E, Lederman D, Hallin E, Sham T K, O'Brien W L and Harp G R 1998 *Phys. Rev.* B **58** 11493
[9] Zitoun D, Respaud M, Fromen M C, Casanove M J, Lecante P, Amiens C and Chaudret B 2002 *Phys. Rev. Lett.* **89** 037203
[10] Berlanga-Ramírez E O, Aguilera-Granja F, Montejano-Carrizales J M, Díaz-Ortiz A, Michaelian K and Vega A 2004 *Phys. Rev.* B **70** 014410
[11] Muñoz Navia M, Dorantes-Dávila J, Respaud M and Pastor G M 2009 *Eur. Phys. J.* D **52** 171
[12] Muñoz Navia M, Dorantes-Dávila J, Zitoun D, Amiens C, Jaouen N, Rogalev A, Respaud M and Pastor G M 2009 *Appl. Phys. Lett.* **95** 233107
[13] Smekhova A, Atamena N, Ciuculescu D, Lecante P, Wilhelm F, Amiens C and Rogalev A 2010 *J. Phys.: Conf. Ser.* **200** 072091
[14] Díaz-Sánchez L E, Dorantes-Dávila J and Pastor G M 2013 *Phys. Rev.* B **88** 134423
[15] Dennler S, Morillo J and Pastor G M 2003 *Surf Sci.* **532–535** 334
[16] Dennler S, Morillo J and Pastor G M 2004 *J. Phys.: Condens. Matter* **16** 2263
[17] Lv J, Zhang F Q, Xu X H and Wu H S 2009 *Chem. Phys.* **363** 65
[18] Lv J, Jia J F, Xu X H and Wu H S 2012 *Physica* B **407** 14
[19] Dieleman D *et al* 2015 *Phys. Chem. Chem. Phys.* **17** 28372
[20] Sessi V, Kuhnke K, Zhang J, Honolka J, Kern K, Tieg C, Šipr O, Minár J and Ebert H 2010 *Phys. Rev.* B **82** 184413
[21] Senf F *et al* 2001 *Nucl. Instr. Meth.* A **467–468** 474
[22] Lau J T, Achleitner A, Ehrke H U, Langenbuch U, Reif M and Wurth W 2005 *Rev. Sci. Instrum.* **76** 063902
[23] Cheng H P and Landman U 1993 *Science* **260** 1304–7
[24] Bromann K, Félix C, Brune H, Harbich W, Monot R, Buttet J and Kern K 1996 *Science* **274** 956–8
[25] O'Brien W L and Tonner B P 1994 *Phys. Rev.* B **49** 15370
[26] O'Brien W L, Droubay T and Tonner B P 1996 *Phys. Rev.* B **54** 9297
[27] Lau J T, Wurth W, Ehrke H U and Achleitner A 2003 *Low Temp. Phys.* **29** 223
[28] Chen K, Beeck T, Fiedler S, Baev I, Wurth W and Martins M 2016 *Phys. Rev.* B **93** 144421
[29] Glaser L, Chen K, Fiedler S, Wellhöfer M, Wurth W and Martins M 2012 *Phys. Rev.* B **86** 075435
[30] de Groot F M F, Abbate M, van Elp J, Sawatzky G A, Ma Y J, Chen C T and Sette F 1993 *J. Phys.: Condens. Matter* **5** 2277
[31] Regan T J, Ohldag H, Stamm C, Nolting F, Lüning J, Stöhr J and White R L 2001 *Phys. Rev.* B **64** 214422
[32] Imperia P, Glaser L, Martins M, Andreazza P, Penuelas J, Alessandrovic V, Weller H, Andreazza-Vignolle C and Wurth W 2008 *Phys. Status Solidi* a **205** 1047
[33] Hirsch K, Lau J T, Klar P, Langenberg A, Probst J, Rittmann J, Vogel M, Zamudio-Bayer V, Möller T and von Issendorff B 2009 *J. Phys. B: At. Mol. Opt. Phys.* **42** 154029
[34] Reif M, Glaser L, Martins M and Wurth W 2005 *Phys. Rev.* B **72** 155405
[35] Sebetci A 2012 *J. Magn. Magn. Mater.* **324** 588
[36] Mokkath J H 2014 *J. Magn. Magn. Mater.* **349** 109
[37] Thole B T, Carra P, Sette F and van der Laan G 1992 *Phys. Rev. Lett.* **68** 1943–6
[38] Carra P, Thole B T, Altarelli M and Wang X 1993 *Phys. Rev. Lett.* **70** 694–7
[39] Lehnert A, Dennler S, Błński P, Rusponi S, Etzkorn M, Moulas G, Bencok P, Gambardella P, Brune H and Hafner J 2010 *Phys. Rev.* B **82** 094409
[40] Lounis S, Reif M, Mavropoulos P, Glaser L, Dederichs P H, Martins M, Blügel S and Wurth W 2008 *Europhys. Lett.* **81** 47004
[41] Bezerra-Neto M M, Ribeiro M S, Sanyal B, Bergman A, Muniz R B, Eriksson O and Klautau A B 2013 *Sci. Rep.* **3** 8